nature climate change

SUPPLEMENTARY INFORMATION

DOI: 10.1038/NCLIMATE3085

Climate change unlikely to increase malaria burden in West Africa

Supplementary Methods

Environmental data inputs for HYDREMATS simulations

Environmental data inputs used for this study are summarized in Supplementary Table 4. We used high-resolution satellite observations of rainfall from the Climate Prediction Center Morphing Technique (CMORPH) Version 1.0 data set, which gives ~8km resolution rainfall data every 30 minutes[1], and has been found in multiple comparison studies to be one of the most skilled satellite rainfall products currently available[2]. CMORPH data is created by combining images from multiple passive microwave sensors, and interpolating them forward and backward in space and time based on cloud advection vectors calculated from geostationary infrared sensors[1].

Like most satellite products, CMORPH is known to have a positive bias compared to rain gauge data in West Africa, primarily due to overestimation of high-intensity rainfall[3]. However, after a simple bias correction, CMORPH can be used as an input to HYDREMATS to accurately simulate the hydrological variables relevant to malaria transmission[4]. We used a probability matching technique[5] so that the cumulative distribution function (CDF) of corrected hourly CMORPH data matched that of the ground observations. Variations of this technique have recently been used to correct biases in CMORPH using rain gauge data[6,7].

We downloaded temperature, wind speed, wind direction, and radiation data for the HYDREMATS simulations from the ERA Interim data set[8] (downloaded from http://www.ecmwf.int/en/research/climate-reanalysis/era-interim). We assumed uniform climatic conditions within the 0.75 degree ERA grid cell. We converted ERA-interim wind speed data from a 10-meter elevation to a 2-meter elevation for use in HYDREMATS by using a logarithmic profile. Also, we linearly interpolated the

ERA-Interim data from the provided 3-hour resolution to a 1-hour resolution as required by HYDREMATS.

We assigned the dominant vegetation type at each location using the University of Maryland Land Cover Classification[9], and assigned soil properties using the Harmonized World Soil Database[10]. We represent soil crusting in the model using a thin layer of low-permeability soil as is typical in West Africa under cultivated conditions[11]. Because this study focuses on climate variables, we held topography constant between locations and assumed that Banizoumbou, Niger topography represents typical topographical conditions and housing patterns in the West Africa Sahel[12].

Downscaling and bias correction of climate change projections

The methodology that we use to downscale GCMs predictions of changes in rainfall and temperature is based on two assumptions that are rooted in the conclusions of previous studies:

(A) The GCMs have limited accuracy in simulating the current and future climate of West Africa [13-15]. In particular the GCMs have poor accuracy in simulating the temporal patterns of rainfall at the daily timescale[16]. As a result, we only use the GCMs simulations to extract information about future changes in (i) annual rainfall magnitude; and in (ii) seasonal distribution of temperature;

(B) The temporal rainfall patterns, at time scales from minutes to weeks, are critically important to the formation of the water pools, the main breeding sites for mosquitos[17]. The physical and biological relationships that shape pool formation, and mosquito population dynamics are highly non-linear. It is not trivial how to average these strongly non-linear relationships form small scales (1 hour, 10 m) to large scales (months, 10 kilometers)[18]. This is why in the simulations presented in this paper, our malaria transmission simulations are carried at the resolutions of 1 hour, 10 meters. As a result, the patterns of rainfall used to force the model has to be realistic, consistent with observations, and we cannot simply use the typically erroneous temporal patterns simulated by climate models.

Based on these assumptions and discussion, we apply the following methodology in describing the forcing of our simulations:

(1) The magnitude of the average change in daily temperature is estimated from the GCM simulations for each month of the year and for each location (x1,y1). This estimated change is then added uniformly to the observed time series from ERA interim reanalysis data set, with 3-hour temporal resolution and 2.5 degrees spatial resolution, at (x1,y1), as a straightforward delta method approach[19-21] . The resulting time series is used to represent the future temperature at (x1,y1).

(2) The relative change in magnitude of the annual rainfall, under future climate conditions, is estimated from the GCM simulations for each location (x1,y1). This relative change is multiplied by the actual observed annual rainfall at (x1,y1), in order to estimate the projected future annual rainfall at (x1,y1). As a variation on the delta method, rather than multiplying our daily or hourly precipitation time series by the delta value, we instead chose the closest location (x1,y2) where the annual rainfall under the current climate, based on observed satellite data that has 8 km resolution, ***is equal to*** the projected future rainfall at (x1,y1) is identified. The satellite-based time series, at 30 minutes resolution, at (x1,y2) is assumed to represent the future rainfall time series at location (x1,y1). For most cases, (x1,y2) is located within about 100 kilometers north or south of (x1,y1), ie. within the same ERA interim grid point.

This approach has the advantage of removing GCM bias, while retaining fine-scale spatial and temporal variability of historical rainfall and temperature [19]. The disadvantage is that the method does not account for changes in rainfall and temperature distributions around the mean. This may be problematic, especially in the case of extreme events such as floods or droughts, which are important for water pool formation, and very high temperatures, which affect mosquito survival. This method also neglects changes to the West African monsoon, which have been shown in recent studies to occur in climate models as a result of several competing physical responses to climate change including an enhanced convective barrier in the pre-monsoon months, enhanced monsoon flow due to greater differential in land-sea temperatures, and vegetation feedbacks [22-25]. The effects of these mechanisms lead to projected decreases in rainfall during the monsoon onset, followed by increased precipitation later in the wet season [22-25]. The timing of the switch between the negative to positive rainfall anomaly was shown to determine the overall changes to total rainfall and length of rainy season, and remains highly uncertain [23]. Such effects can impact malaria transmission, particularly if they alter the duration of the rainy season, as this would in turn alter the length of the malaria transmission season. Changes to the frequency and intensity of rainfall events within the rainy season could also have important impacts, as these affect water pool persistence and play a large role in determining the malaria response to rainfall [17].

Supplementary Discussion

Comparison of simulated variables to observational data

HYDREMATS has previously undergone extensive validation in two villages in Southern Niger[26-28]. Data sampling locations in one of the villages, Banizoumbou, are shown in Supplementary Fig. 2. Environmental data collected included one-hour resolution meteorological variables, spatially distributed soil, vegetation and topography values, and time-varying measurements of soil moisture, and the depths and temperatures of selected recurring water pools. Entomological variables collected included adult mosquitoes captured in CDC light traps and mosquito larvae collected using a standard dipping method[26,27]. Bimonthly blood samples were taken from children aged one through five years old[28]. We demonstrated the model's ability to simulate hydrology, entomology and malaria prevalence in this region[26-28].

Here, we present additional model validation, through a comparison of simulations to observations from three other sources: the Beier data set on EIR and malaria prevalence[29], malaria prevalence estimates from the Malaria Atlas Project[30], and entomology and malaria prevalence data from the Garki district in Nigeria[31].

Comparison to Beier data

Beier et al.[29] compiled paired data from 31 locations across Africa and developed a relationship between the entomological inoculation rate (EIR), and malaria prevalence. These paired data points originated from multiple countries including Kenya, Ethiopia, Tanzania, Republic of Congo, Burkina Faso, and Senegal, spanning a wide range of climate zones. The paired data points were selected by conducting a literature search with the following inclusion criteria: entomological data collected over at least one year with a minimum of monthly sampling over the transmission season, standard methods for estimating mosquito densities and sporozoite rates, and no vector control interventions. Inclusion criteria for the prevalence data included use of standard blood smear techniques and reporting by time period and age group. In instances where the original malaria prevalence data were reported for multiple time periods and age groups, the single highest prevalence value was selected. The analysis showed a linear relationship between prevalence and the logarithm of annual EIR. This log-linear relationship persisted when data were stratified by ecological zone as well as between East and West Africa, indicating that this is a fundamental relationship and independent of climate. These data therefore provide a test for the human immunity and malaria transmission component of HYDREMATS, which has been less extensively tested against observations than the hydrology and entomology components.

Because Beier et al. used the maximum prevalence value sampled over multiple age groups and time periods, we compared the data to the maximum simulated prevalence for the 2 to 10 year age group from our equilibrium simulations. HYDREMATS was able to reproduce the observed log-linear relationship between EIR and peak malaria prevalence (Figure 2, main text). Our simulation results and observational data agree very well for a wide range of epidemiological conditions, from 0 to over 300 infectious bites per person per year.

Comparison to data from the Malaria Atlas Project

The Malaria Atlas Project (MAP), based at the University of Oxford, produces maps showing global estimates of various measures of malaria risk. MAP compiles and maintains a database of routine malaria prevalence surveys. The current maps use over 22,000 geo-referenced data points of malaria prevalence measured between 1985 and 2010 from across the 85 malaria endemic nations and standardized to the 2 to 10 year old age group[30]. Temperature and aridity masks are used to predict the limits of stable malaria. Within the predicted limits of stable malaria transmission, these prevalence data are mapped to a global surface at a 5 km x 5km resolution using Bayesian inference and geospatial modeling[30]. The MAP estimate of malaria prevalence in children aged 2 to 10 years is shown as the colored surface in Supplementary Fig. 3, top panel. The colors of the overlaying circles show the prevalence during the peak malaria transmission season simulated by HYDREMATS in the equilibrium simulations.

Supplementary Fig. 3, bottom panel, compares simulated peak prevalence to the MAP estimate, with results of the equilibrium simulation on the right, and the mean of the multiyear simulation on the left. For the majority of the twelve locations, simulated results match well with the MAP estimate. One outlier in the equilibrium results is the point S1, located in Senegal. This could be explained in part by Senegal's malaria control activities, which cause observed prevalence to be substantially lower than what would have been expected given the environmental conditions. Our simulations did not account for varying levels of malaria control between locations. Inter-annual variability is likely playing a role as well, as the MAP estimates do not address seasonal and inter-annual variability in response to climate. Another discrepancy between simulations and MAP estimates are the three locations (N1, N2 and M3) where simulated prevalence was 0%, while MAP estimates levels between 10 and 30%. There are several additional explanations for this discrepancy. One is that in the sparsely populated regions of northern Niger and Mali, there are very few observations of malaria prevalence. In these regions, MAP estimates rely on statistical techniques using environmental covariates including rainfall, temperature, land cover, and rural versus urban classification. We therefore have less confidence in MAP estimates at high latitudes. Another explanation for the discrepancy is that while the equilibrium simulation predicted R_0 less than one leading to elimination of the parasite, all three of these locations had at least some years with R_0 greater than one. Transmission is therefore possible in these locations if the parasite is present in the population during years with R_0 greater than one. A third possibility for the discrepancy is that these locations may have had some form of permanent water source not accounted for in our simulations that could serve as mosquito breeding habitat in the absence of rain-fed water pools, such as oases. This is likely to be true of M3, which lies on the banks of a tributary to the Niger River.

Comparison to data from the Garki Project

The Garki Project was a major effort to study malaria transmission and control by the World Health Organization and the Government of Nigeria from 1969 to 1976. The study location corresponds with site NA1 shown in Fig. 1 in the main text. The goals of the project were to study the epidemiology of malaria transmission in the Sudan Savanna climate zone, test intervention methods, and develop a model of disease transmission[31]. The study included four tiers of villages. Malaria control interventions were applied to the inner villages. Villages outside of the intervention zone were monitored as non-intervention comparison locations. Mosquitoes were captured every 5 weeks during the dry season and every 2 weeks during the wet season using human landing catches. Human bait collectors were stationed at indoor and outdoor locations for the duration of the night and collected mosquitoes attempting a blood meal. Mosquitoes were also captured using pyrethrum spray collections and light traps. Captured mosquitoes were counted and analyzed in order to estimate the mosquito biting rate, EIR, mosquito age, and the sporozoite rate (proportion of mosquitoes infected by the *plasmodium* parasite). Age-specific malaria prevalence was measured for selected villages every 10 weeks using standard blood smear methods. Seroimmunological surveys were conducted every 6 months to test for the presence of antibodies to *Plasmodium falciparum* and other forms of the malaria parasite within the human population.

Supplementary Fig. 4 shows a comparison between data on mosquito biting rates collected from Kwaru village outside of the intervention area and the corresponding variable simulated by HYDREMATS in our 15-year baseline simulation. Because the high-resolution environmental data sources required for HYDREMATS simulations did not overlap with the Garki Project time period, we compared the results to the range of values simulated in our 15-year simulation. As shown in the figure, the model reproduces the general characteristics and timing of the seasonal cycle. Our simulation results show mosquito biting activity to be restricted to the period between May and early November, corresponding to the availability of rain-fed water pools required for mosquito breeding. The observations show occasional mosquito bites outside of this period; these may have been mosquitoes that had taken refuge inside of homes, or were engaging in low-level localized breeding in a permanent water source not represented in our model. Our simulations also include low levels of mosquitoes to sustain the mosquito population over the dry season; however, these mosquitoes are assumed to enter an aestivation state and do not engage in blood seeking activity until the beginning of the following wet season[32].

The top panel in Supplementary Fig. 5 shows prevalence by age for a cross-section of the population in the non-intervention villages measured in October, 1971, at the end of rainy season. The observations, in red, show a characteristic age profile of malaria prevalence. Young children become infected at high rates until they begin to develop partial immunity to disease. This explains the sharp decrease in prevalence between the first few years of life and early adolescence. While the exact shape and magnitude of the prevalence profile varies by year and by location, HYDREMATS succeeds in simulating the basic characteristics of the age profile. In this simulation, children appear to develop immunity several years faster than the observed population.

Finally, the bottom panel of Supplementary Fig. 5 shows the seasonal cycle of malaria prevalence in the Garki district. The red and blue lines show observed prevalence sampled in two non-intervention villages over four years (1971-1974), and simulated prevalence in the same area between 1998 and 2012. While the specific prevalence value varies from year to year, HYDREMATS correctly simulates the timing of the seasonal peak around early October, and simulates reasonable levels of prevalence.

The simulations showed much higher interannual variability than the observations. However, the observations span only four years, with relatively low and stable rainfall (between 300-600 mm / year). By contrast, mean annual rainfall between 1998-2012 was 765 mm, with a standard deviation of 168 mm, and as much as 586 mm difference between consecutive years. It is therefore not unreasonable that we should see such high variability in simulated malaria prevalence over this time. Our simulations also tend to underestimate malaria prevalence in the dry season. One possible explanation for this is that our simulated population had higher immunity levels than the observed population, causing infections to clear more rapidly. There was also evidence of low levels of malaria transmission occurring during the dry season, which generally did not occur in the model simulations [31].

Regression relationships between climate and malaria transmission indices

We developed a linear regression model for each of the malaria transmission indices. We broke annual rainfall into segments that accounted for threshold effects and other nonlinearities between rainfall and predictor variables. For R_0, the slope of the least-squares regression line was greater for annual rainfall values less than 690 mm than it was for higher values. In years with rainfall less than 690mm, mosquitoes were constrained by the availability and persistence of sufficiently persistent developmental habitats. Additional rainfall made it more likely that a water pool will last long enough for larvae to emerge as adults, thus increasing R_0. In years with heavy rainfall, mosquitoes had many water pools available for breeding, so the abundance was less sensitive to increases in rainfall. Excess rainfall can lead to pools that are too deep for *Anopheles gambiae s.l.* mosquitoes, which prefer to breed in shallow areas. Larval mosquito abundance is also regulated by the carrying capacity of developmental habitats in years with ample rainfall and density-dependent mortality.

The relationship between rainfall and EIR had two distinct segments. Rainfall was linearly correlated to the logarithm of EIR for annual rainfall up to 950 mm. Beyond this threshold, the two were no longer correlated, both because of the waning influence of rainfall on mosquito numbers at high rainfall, and also because prevalence did not increase with rainfall beyond this point.

The influence of rainfall on prevalence and the immunity index had three distinct segments. For rainfall values less than 415 mm per year, environmental and entomological conditions were generally insufficient to sustain transmission, resulting in near-zero values of EIR. There was a loose linear relationship between rainfall and malaria indices for annual totals between 415 mm and 950 mm. There was almost no correlation between rainfall greater than 950 mm and malaria transmission, due to the finite number of susceptible individuals, the upper limit of acquiring immunity, and the decreased sensitivity of mosquitoes to high levels of rainfall.

Sensitivity of results to climate change projections

We investigated the sensitivity of our results to the choice of climate change projections by 1) extending our modeling study to include two additional GCMs: CanESM2 and MIROC5 and 2) demonstrating how Fig. 4 (main text) can be used to estimate the sensitivity of results to differences in climate projections

1) In addition to the two GCMs used in our study (CCSM4 and MPI-ESM-MR), we conducted simulations using two additional GCMs to investigate the sensitivity of our results to the choice of climate projection. The four models show a general pattern of drying in the western portion of our study area, and wetting in the eastern and southern areas (Supplementary Fig. 7). The magnitude of these changes, as well as the extent of the area with predicted drying, varies by model. This pattern of rainfall change is consistent with a substantial majority of CMIP5

models and has been identified as a robust feature of future climate in this region [14,24,33,34].

Temperatures generally increase more in the west than in the east, consistent with the spatial extent of predicted changes in precipitation (Supplementary Fig. 8). The four-model mean shows temperature increases between 2.5 and 5.8 degrees Celsius of our study area. MIROC5 and CCSM4 are substantially cooler than the mean, while CanESM2 projects temperature increases over 8 degrees Celsius in the western Sahel.

MIROC5 is known to produce one of the coolest and wettest projections over the Sahel (Subregions ii and iii) within the CMIP5 ensemble; most CMIP5 models project higher temperatures, and rainfall within 30% of current values[14]. In this regard, our simulations results from MIROC5 can be seen as a worst-case scenario in terms of potential increases in malaria transmission. By contrast, CanESM2 shows a considerably stronger drying and warming signal than the other three models. The results of our simulations using all four climate models are shown in Table 4.

2) The uncertainty in climate projections was a motivating factor in our development of the relationships linking rainfall and temperature to malaria transmission indices, which use simulations driven by over one thousand combinations of annual climate data to explore a wide range of temperature and rainfall conditions that may be observed in this region. The resulting plots shown in Fig. 4, as well as the regression equations outlined in the Supplementary materials, can be used to estimate the effects of different climate change scenarios on malaria transmission throughout this region.

In Supplementary Fig. 10, we show the current and future values of mean annual rainfall and wet-season temperature, superimposed on the scatterplots of malaria transmission indices in rainfall-temperature space shown in Fig. 4. The yellow points show the current climate, and the green points show the future climate as projected by each of our four climate models. The sensitivity of our results to climate projections can be estimated by considering the spread of the green points, and the values of R_0 and malaria prevalence in the underlying scatterplots. This method can also be used to estimate the climate change impacts on malaria transmission for additional locations within study area, as well as the impacts of different climate projections. Most significant would be changes that cause the movement from the high transmission (red) to low transmission (blue) regions of rainfall-temperature space. It is important to note that while each location is shown as a single point, in reality we would observe a cloud of points surrounding the mean due the high interannual variability in rainfall and temperature, as shown in Fig. 3b and 3c.

In Sub-region i, both increased temperature and decreased rainfall work to reduce malaria transmission. A future climate that was substantially wetter could potentially lead to increases in malaria prevalence; however, such a future is unlikely given the near-consensus of current generation climate models of a dryer future in this region [14].

In Sub-region ii, any future warming leads to conditions that exceed the limits of mosquito survival; no amount of additional rainfall could make this area suitable for malaria transmission.

As stated in the main text, future malaria transmission is most uncertain in Sub-region iii, due to the competing forces of increased mosquito breeding through higher rainfall and shorter mosquito lifespan through increased temperatures. Furthermore, this region sits close to the threshold of malaria transmission; small changes can push the system in or out of the epidemic region. This region is therefore the most sensitive to the selection of climate projections. In our simulation results, the relatively cool and wet future predicted by MIROC5 led to increased prevalence at site N2.

Finally, Sub-region 4 is currently deep in the high-transmission area of rainfall-temperature space. Modest changes in climate are not sufficient to significantly change frequency or severity of epidemics. However the very strong drying and warming signal predicted by CanESM2 was enough to cause a significant decrease in malaria prevalence.

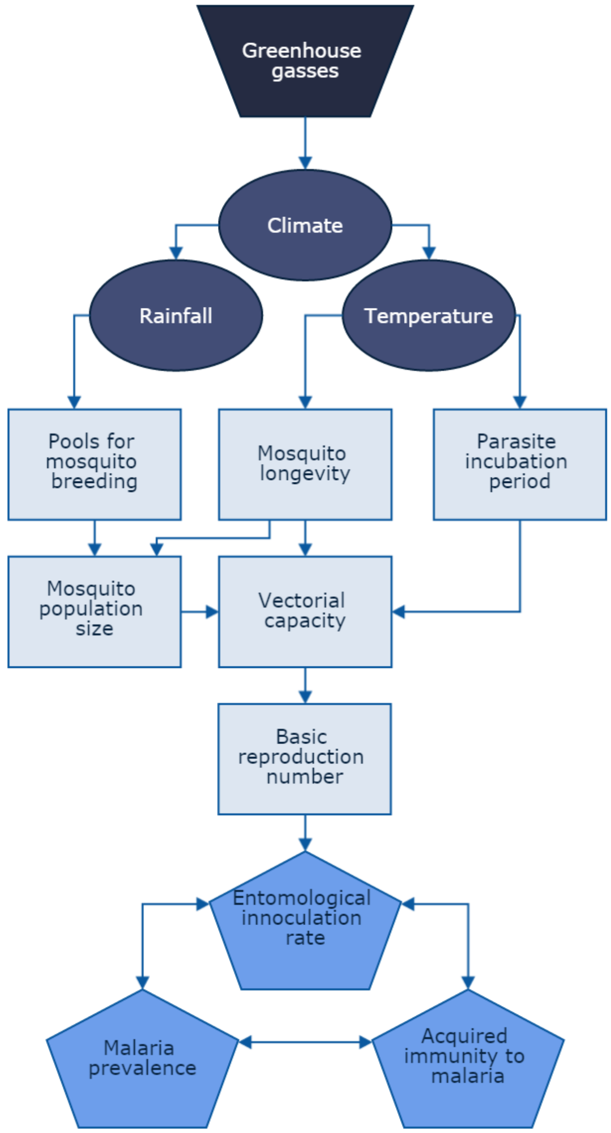

Supplementary Figure 1
Schematic of the processes linking climate change to malaria transmission. Rainfall primarily affects mosquito breeding, while temperature affects mosquito longevity and parasite development rate.

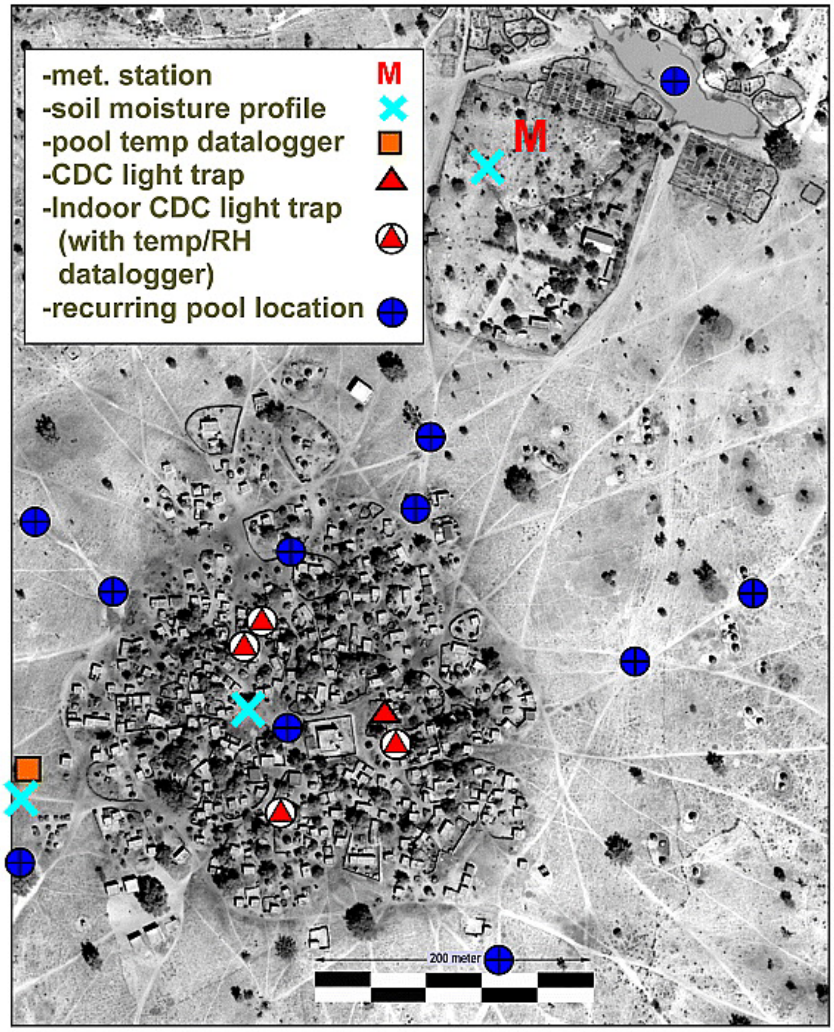

Supplementary Figure 2
Data sampling locations in Banizoumbou, Niger. Reprinted from Bomblies et al[26]. The hydrology component of HYDREMATS was rigorously compared to field observations in Bomblies et al[26], showing that the model very closely reproduced observed volumetric water content is soil, as well as location, depth and persistence of water pools.

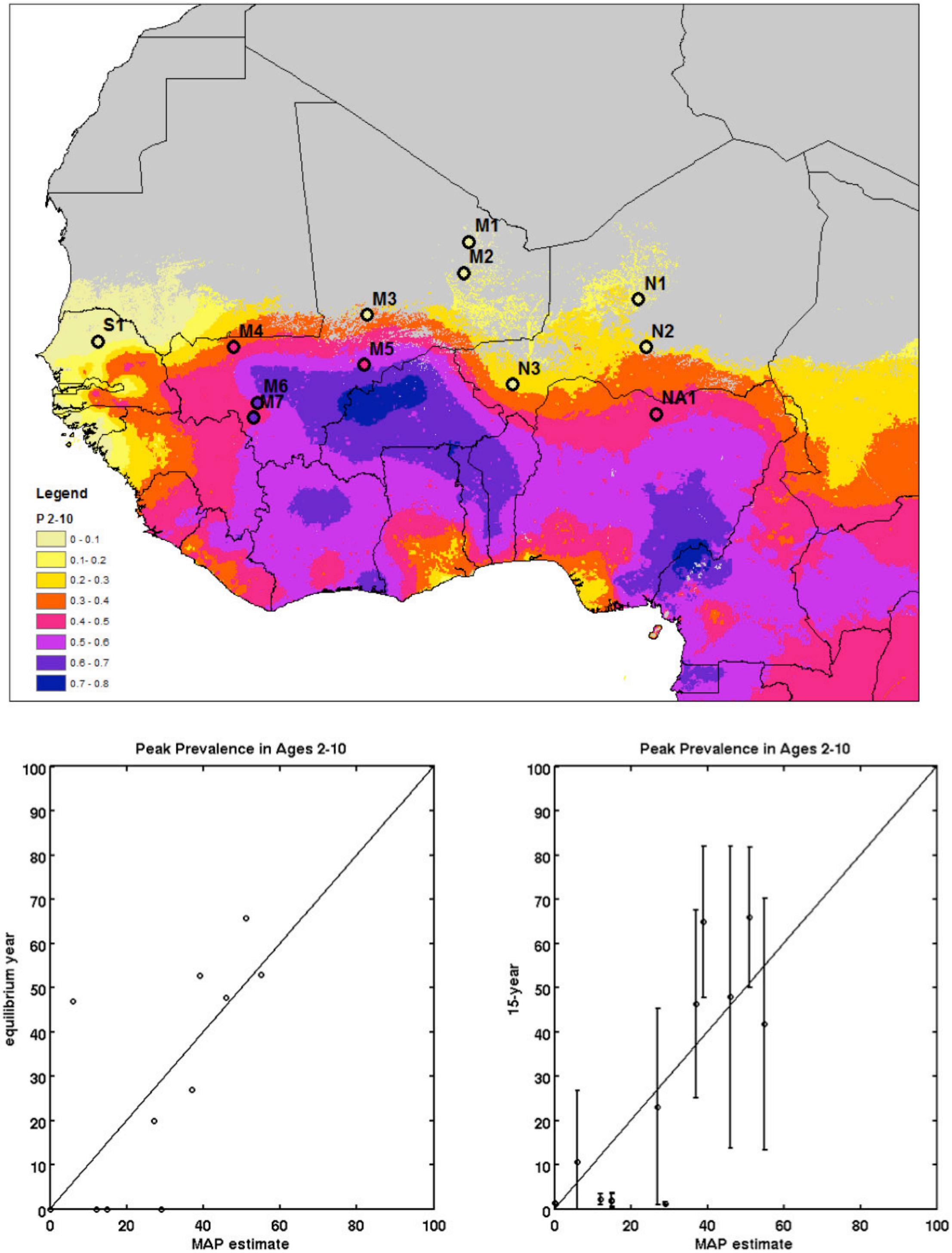

Supplementary Figure 3

Top: Malaria prevalence in children aged 2-10 in 2010 estimated by Malaria Atlas Project [30] (colored surface) and peak equilibrium prevalence simulated by HYDREMATS (colored circles). Bottom left: Simulated prevalence in children aged 2-10 for equilibrium simulation compared to MAP estimate. Each point refers to one of the twelve locations in the top panel. Bottom right: Simulated prevalence in children aged 2-10 over a 15-year simulation. Error bars on for the 15-year simulation show one standard deviation from the mean.

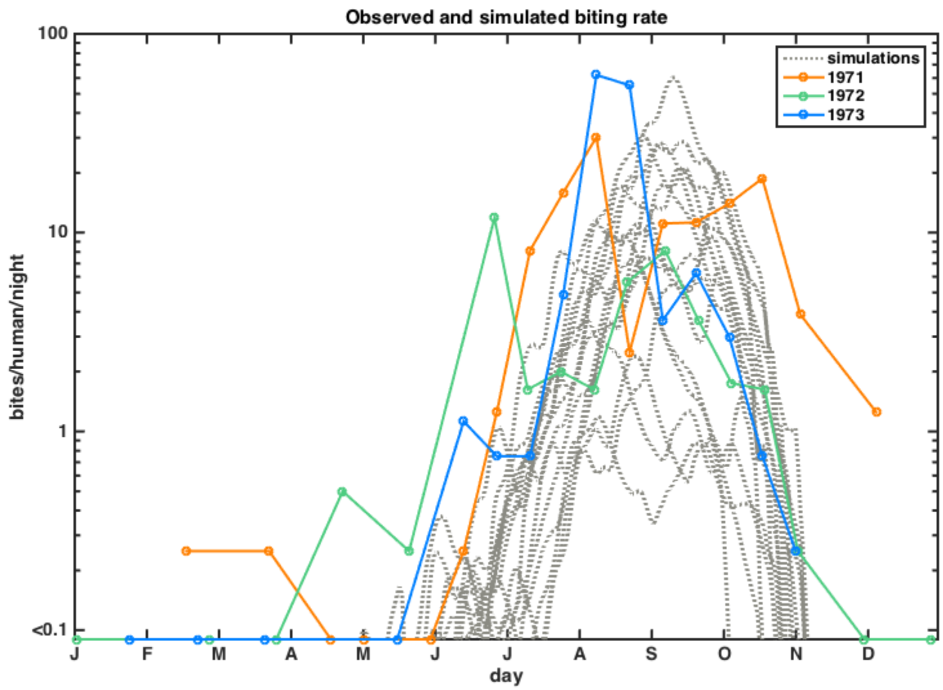

Supplementary Figure 4
Mosquito biting rate in Kwaru, Nigeria, one of the non-intervention comparison villages in the Garki project[31]. Colored lines show captured mosquitoes for 3 consecutive years. Grey lines show simulation results.

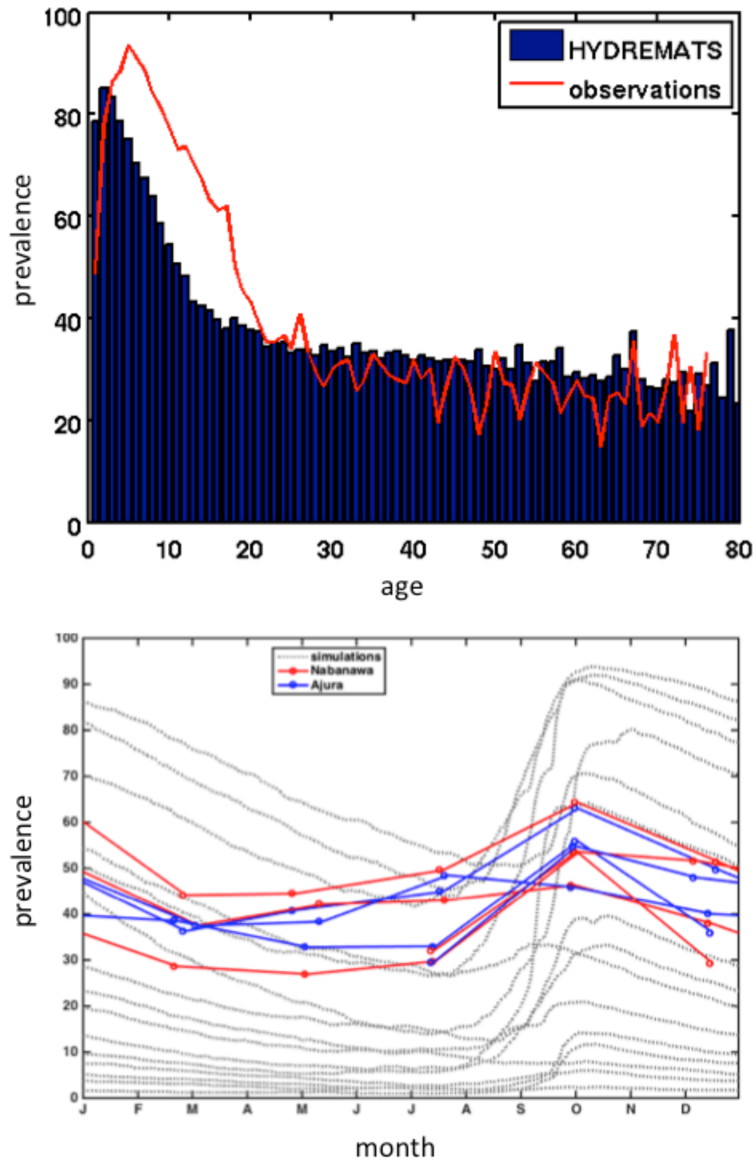

Supplementary Figure 5
Top: Malaria prevalence by age group in October, 1971. The observations show that malaria prevalence peaks in childhood and gradually decreases through adolescence, with dramatically lower prevalence rates in adults. This is the result of semi-protective immunity, which is gradually acquired through repeated malaria infections. The blue bars show a cross-section of the simulated model population, showing a similar pattern of prevalence vs. age as older individuals are protected by higher levels of immunity. Bottom: Observed and simulated seasonal cycle of malaria prevalence in the Garki district. Grey lines show simulated malaria prevalence between 1998-2012. The red and blue lines show observed malaria prevalence sampled at two control villages over the period 1971-1974.

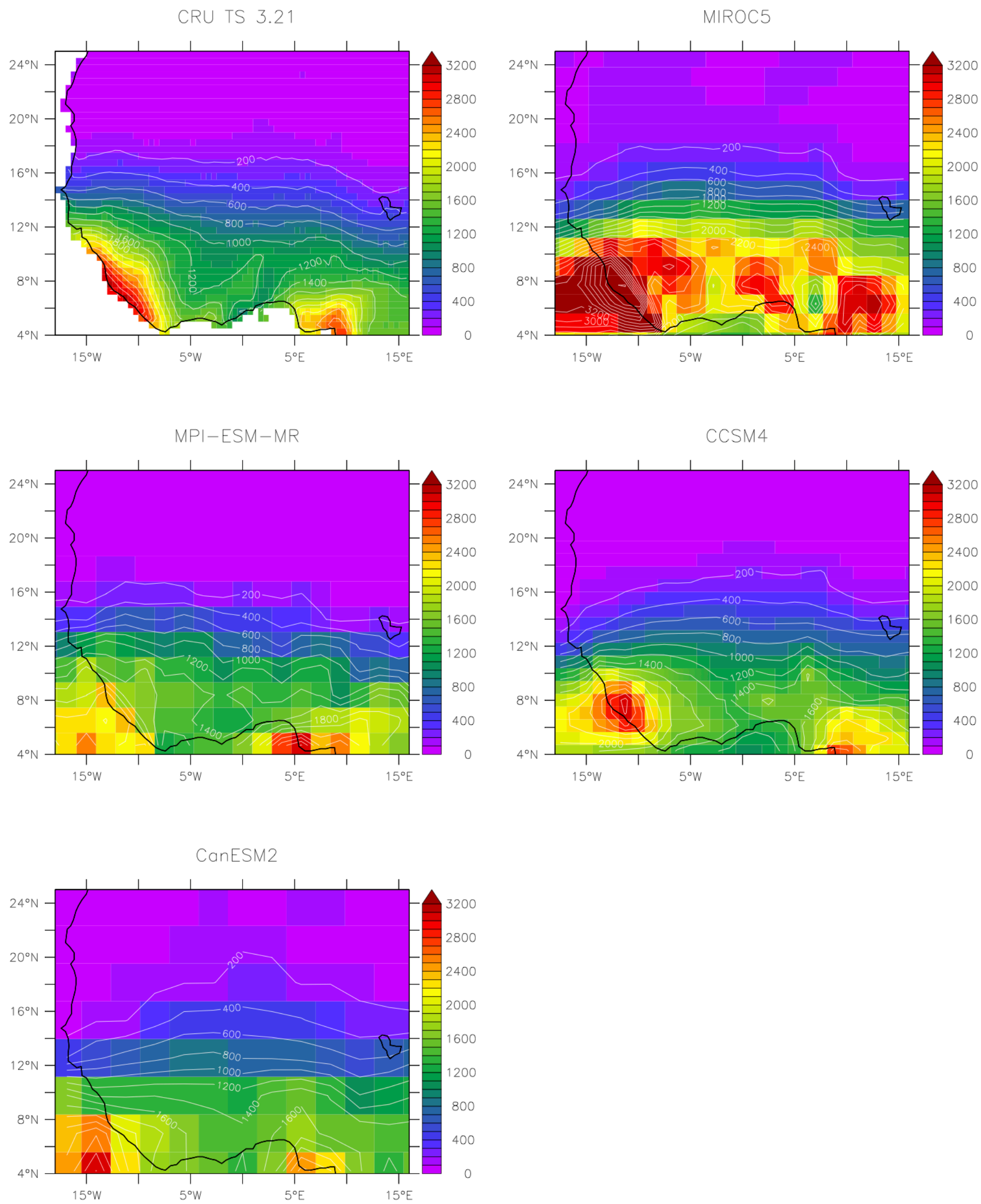

Supplementary Figure 6
Mean annual rainfall [mm] during the period 1930-2005. The top-left panel shows observational data from CRU TS3.21. The remaining panels show rainfall simulated in the historical runs of the four climate models used in this study.

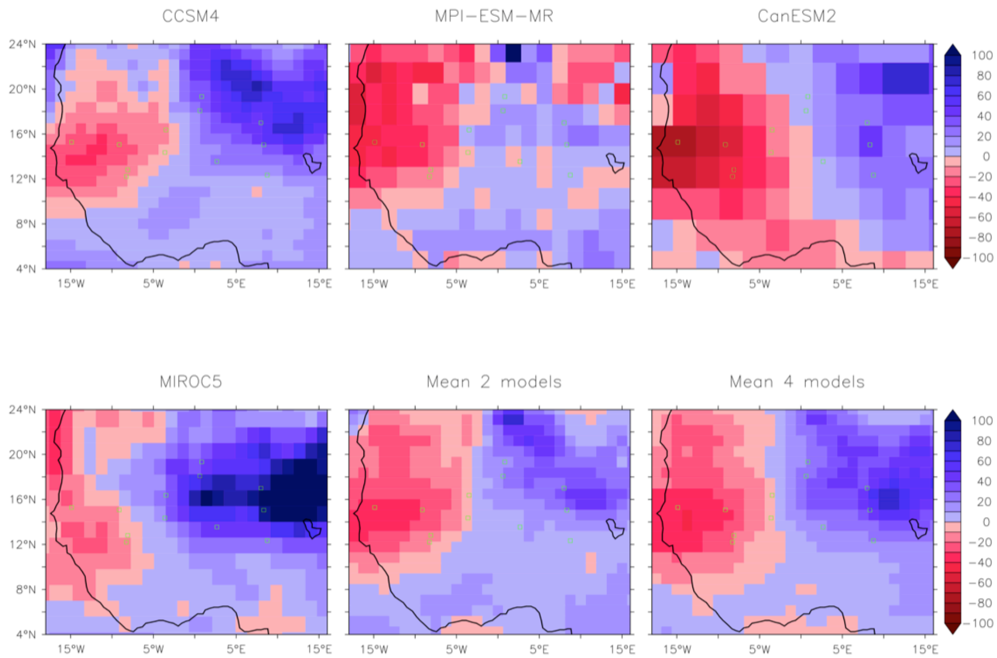

Supplementary Figure 7
Predicted change in rainfall by 2070-2100 as a percentage of 1975-2005 mean rainfall under RCP8.5.
Predictions are shown for the following CMIP5 models: CCSM4, MPI-ESM-MR, CanESM2 and MIROC5. The bottom-center plot shows the percent change averaged between CCSM4 and MPI-ESM-MR models, and the bottom-right plot shows the average prediction over all 4 CMIP5 models.

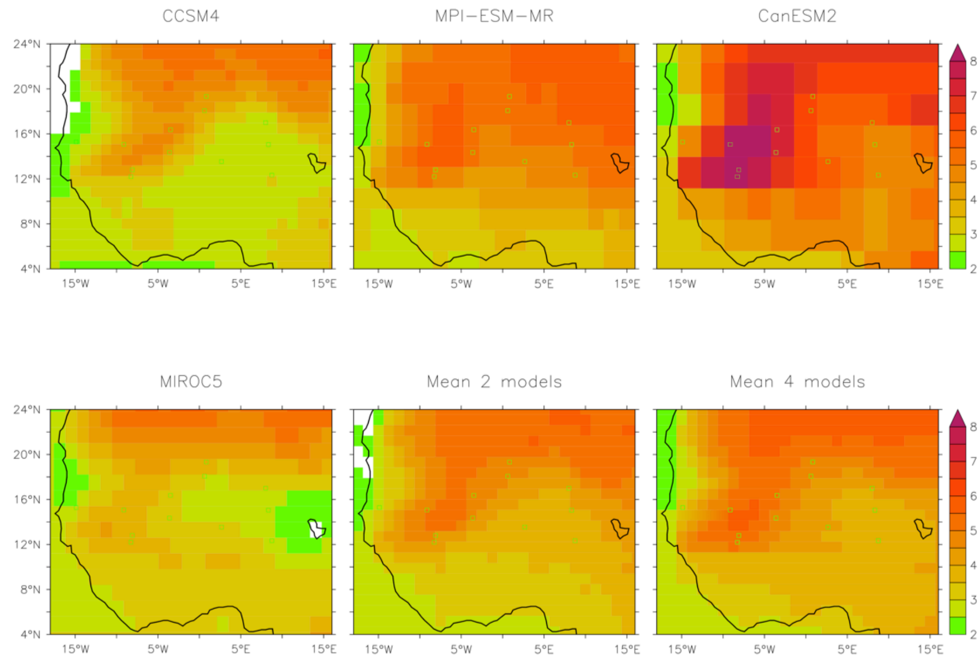

Supplementary Figure 8

Predicted increase in July-August-September mean temperature between 1975-2005 and 2070-2100, in degrees Celsius, under RCP8.5. Predictions are shown for the following CMIP5 models: CCSM4, MPI-ESM-MR, CanESM2 and MIROC5. The bottom-center plot shows the percent change averaged between CCSM4 and MPI-ESM-MR models, and the bottom-right plot shows the average prediction over all 4 CMIP5 models.

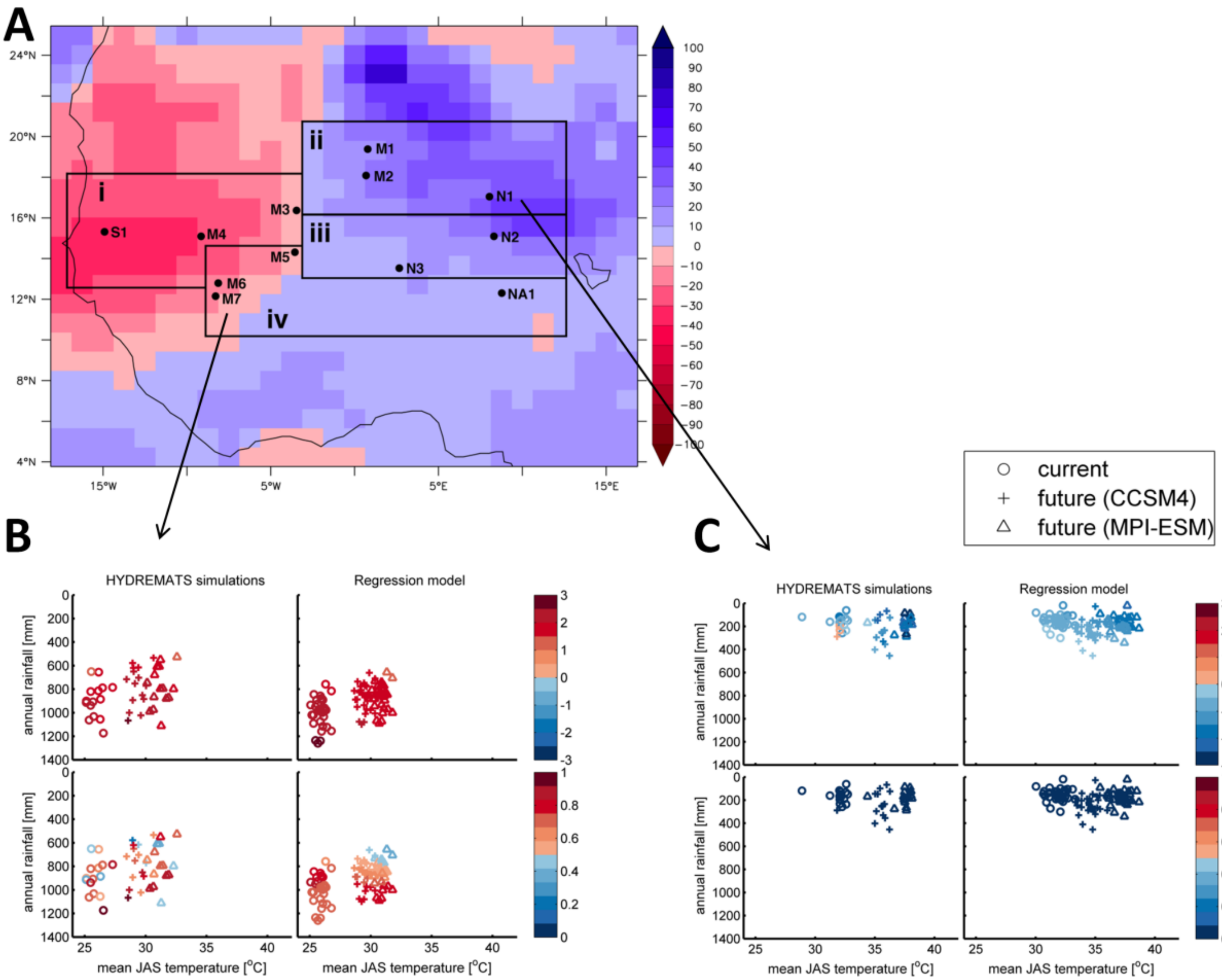

Supplementary Figure 9

A) The colors on the map indicates the changes in average rainfall between current (1975-2005) and future (2070-2100) conditions, averaging predictions between the two climate models. The labeled rectangles group our study area by response to climate change. B and C) Detailed results for observed changes in R_0 and malaria prevalence are shown for two sites, M7 (Fig 3Sb) in the south and N1 (Fig. 3SC) in the north. The top rows show log10 (R_0) and the bottom row shows malaria mean prevalence in children aged 2-10. Open circles indicate model results in the current climate, crosses show results with future climate conditions as predicted by CCSM4 and triangles indicate results using climate predictions from MPI-ESM-MR. The left panels are modeling results from the detailed HYDREMATS simulations. The right panels apply a regression relationship to annual rainfall and mean wet season temperature data from CRU TS3.1.

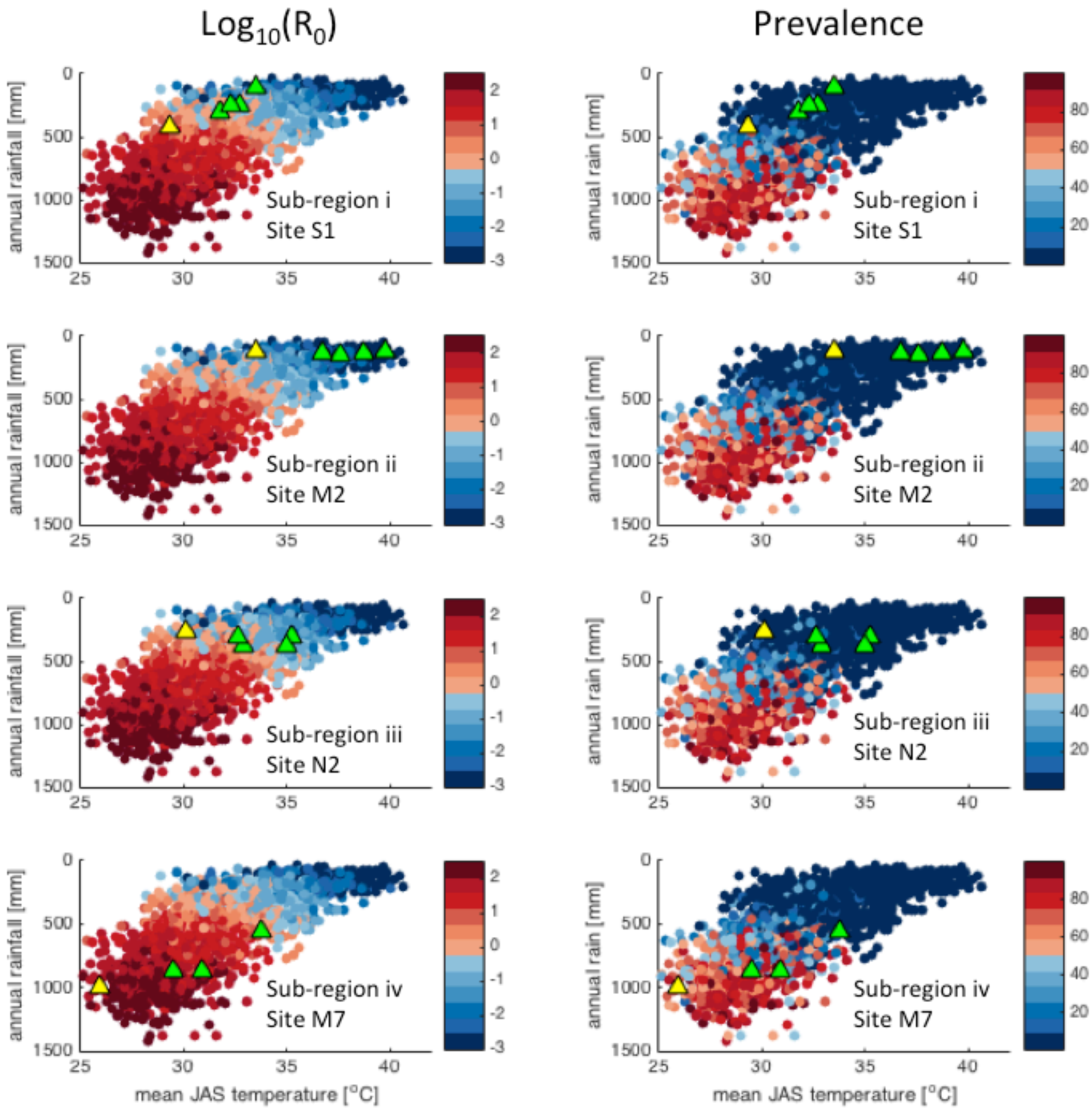

Supplementary Figure 10

Migration of study sites through rainfall-temperature space under different projections of future climate. The triangular markers in each subplot show the location of a study site in rainfall-temperature space under current (yellow) and future (green) conditions under projections from four climate models: CCSM4, MPI-ESM-MR, CanESM2 and MIROC5. The markers are overlaid on plots of log(R0) (left column) and malaria prevalence in ages 2-10 (right column). The spread between green markers estimates the uncertainty in future malaria transmission due to differences in climate projections.

Supplementary Table 1: HYDREMATS simulation results for baseline period (1975-2005) and future conditions (2070-2100). We show results for simulations using climate projections from the two GCMs selected for our study (CCSM4 and MPI-ESM-MR), as well as two additional models as a sensitivity analyses (CanESM2 and MIROC5). Red values indicate statistically significant decreases from baseline while green values indicate statistically significant increases.

Proportion of years with R0 > 1 (95% CI)

Sub-region	Site	Base	CCSM4	MPI-ESM-MR	CanESM	MIROC5
i	M3	0.20 (0.04,0.48)	0.00 (0.00,0.22)	0.00 (0.00,0.22)	0.00 (0.00,0.22)	0.27 (0.08,0.55)
i	S1	0.73 (0.45,0.92)	**0.27 (0.08,0.55)**	**0.07 (0.00,0.32)**	**0.00 (0.00,0.22)**	0.40 (0.16,0.68)
i	M4	0.87 (0.60,0.98)	0.53 (0.27,0.79)	**0.33 (0.12,0.62)**	**0.00 (0.00,0.22)**	0.93 (0.68,1.00)
ii	M1	0.00 (0.00,0.22)	0.00 (0.00,0.22)	0.00 (0.00,0.22)	0.00 (0.00,0.22)	0.00 (0.00,0.22)
ii	M2	0.00 (0.00,0.22)	0.00 (0.00,0.22)	0.00 (0.00,0.22)	0.00 (0.00,0.22)	0.00 (0.00,0.22)
ii	N1	0.13 (0.02,0.40)	0.07 (0.00,0.32)	0.00 (0.00,0.22)	0.00 (0.00,0.22)	0.00 (0.00,0.22)
iii	N2	0.53 (0.27,0.79)	0.67 (0.38,0.88)	**0.07 (0.00,0.32)**	0.40 (0.16,0.68)	**1.00 (0.78,1.00)**
iii	N3	1.00 (0.78,1.00)	0.93 (0.68,1.00)	**0.33 (0.12,0.62)**	**0.53 (0.27,0.79)**	1.00 (0.78,1.00)
iv	M5	1.00 (0.78,1.00)	1.00 (0.78,1.00)	1.00 (0.78,1.00)	1.00 (0.78,1.00)	1.00 (0.78,1.00)
iv	M6	1.00 (0.78,1.00)	1.00 (0.78,1.00)	1.00 (0.78,1.00)	1.00 (0.78,1.00)	1.00 (0.78,1.00)
iv	NA1	1.00 (0.78,1.00)	1.00 (0.78,1.00)	1.00 (0.78,1.00)	1.00 (0.78,1.00)	1.00 (0.78,1.00)
iv	M7	1.00 (0.78,1.00)	1.00 (0.78,1.00)	1.00 (0.78,1.00)	1.00 (0.78,1.00)	1.00 (0.78,1.00)

Log_10(R0) (95% CI)

Sub-region	Site	Base	CCSM4	MPI-ESM-MR	CanESM	MIROC5
i	M3	-0.3 (-0.7,-0.0)	**-2.1 (-2.4,-1.7)**	**-1.5 (-1.8,-1.1)**	**-2.4 (-2.7,-2.0)**	-0.2 (-0.4,-0.0)
i	S1	0.7 (0.2,1.1)	**-0.5 (-0.9,-0.0)**	**-1.5 (-2.0,-1.0)**	**-2.8 (-3.0,-2.5)**	**-0.2 (-0.6,0.1)**
i	M4	1.0 (0.7,1.4)	**-0.0 (-0.5,0.5)**	**-0.3 (-0.7,0.1)**	**-2.4 (-2.7,-2.1)**	0.8 (0.5,1.0)
ii	M1	-1.9 (-2.4,-1.4)	**-2.8 (-3.0,-2.6)**	**-3.0 (-3.0,-3.0)**	**-3.0 (-3.0,-3.0)**	**-2.5 (-2.8,-2.2)**
ii	M2	-2.2 (-2.7,-1.7)	-2.7 (-3.0,-2.4)	**-2.8 (-3.0,-2.6)**	**-2.9 (-3.1,-2.8)**	-1.9 (-2.2,-1.6)
ii	N1	-0.7 (-1.1,-0.4)	**-1.3 (-1.7,-0.9)**	**-2.2 (-2.6,-1.7)**	**-2.2 (-2.6,-1.7)**	-0.8 (-1.0,-0.6)
iii	N2	0.0 (-0.3,0.3)	0.2 (-0.2,0.6)	**-0.8 (-1.1,-0.5)**	-0.1 (-0.3,0.1)	**1.0 (0.8,1.3)**
iii	N3	1.0 (0.7,1.3)	0.9 (0.6,1.1)	**-0.2 (-0.5,0.0)**	**-0.1 (-0.4,0.1)**	1.2 (1.1,1.4)
iv	M5	1.6 (1.5,1.8)	1.4 (1.2,1.6)	**1.2 (0.9,1.4)**	**1.2 (0.9,1.5)**	1.5 (1.3,1.6)
iv	M6	2.0 (1.9,2.2)	2.1 (1.9,2.2)	1.9 (1.8,2.0)	**1.5 (1.4,1.6)**	**2.3 (2.2,2.4)**
iv	NA1	1.6 (1.3,1.8)	1.7 (1.6,1.9)	1.4 (1.1,1.7)	1.7 (1.5,1.9)	**2.0 (1.9,2.1)**
iv	M7	1.9 (1.8,2.0)	**2.1 (2.0,2.3)**	1.9 (1.8,2.1)	**1.6 (1.5,1.6)**	**2.4 (2.2,2.5)**

Peak Prevalence in children aged 2-10 (95% CI)

Sub-region	Site	Base	CCSM4	MPI-ESM-MR	CanESM	MIROC5
i	M3	2% (1,3)	3% (2,4)	2% (1,3)	3% (1,5)	3% (1,4)
i	S1	11% (2,20)	**2% (1,2)**	**2% (1,2)**	2% (2,3)	**2% (1,2)**
i	M4	46% (34,58)	**9% (5,14)**	**4% (2,6)**	**9% (5,14)**	**17% (7,28)**
ii	M1	1% (1,1)	1% (1,1)	1% (1,1)	**2% (1,2)**	1% (1,2)
ii	M2	2% (1,3)	2% (1,3)	2% (1,3)	3% (2,5)	2% (1,4)
ii	N1	2% (1,3)	2% (1,3)	2% (1,2)	2% (1,4)	2% (0,4)
iii	N2	2% (1,4)	4% (1,6)	2% (1,4)	4% (0,8)	**19% (8,29)**
iii	N3	23% (11,35)	13% (10,16)	**4% (2,6)**	**4% (0,8)**	26% (19,33)
iv	M5	42% (26,57)	43% (26,60)	30% (13,47)	27% (8,46)	29% (18,40)
iv	M6	66% (57,75)	67% (59,76)	64% (55,74)	**33% (18,48)**	69% (61,78)
iv	NA1	48% (29,67)	66% (52,80)	54% (38,70)	55% (38,71)	66% (51,80)
iv	M7	65% (55,74)	67% (57,78)	66% (57,76)	**35% (19,51)**	69% (59,79)

Supplementary Table 2: Coefficient of determination (R^2) values for annual rainfall, TJAS and indices of malaria transmission

	TJAS	$\log_{10}$ (R0)	$\log_{10}$ (EIR)	Pr 2-10	Imm
Annual rainfall	0.51	0.72	0.81	0.62	0.68
TJAS		0.67	0.64	0.52	0.42
$\log_{10}$ (R0)			0.87	0.51	0.53
$\log_{10}$ (EIR)				0.7	0.81
Pr 2-10					0.65

All pairs of variables are correlated with significance levels $p << 0.0001$

Supplementary Table 3: Coefficients and statistics of regression model.

Regression models take the form of f(TJAS,rain)=a+b*TJAS+c*rain/1000

	Breakpoint	a (95% CI)	b (95% CI)	c (95% CI)	R^2 for segment	p-value	R^2 overall	RMSE
$\log_{10}$ R0 (unitless)	rain < 690 mm	4.00 (3.44,4.57)	-0.17 (-0.18,-0.15)	3.76 (3.53,4.00)	0.72	<0.0001	0.85	0.41
	rain > 690 mm	3.03 (2.54,3.53)	-0.08 (-0.09,-0.06)	1.20 (1.02,1.37)	0.44	<0.0001		
$\log_{10}$ EIR (unitless)	rain < 950 mm	1.77 (1.17,2.37)	-0.14 (-0.16,-0.12)	3.51 (3.33,3.70)	0.75	<0.0001	0.8	0.55
	rain > 950 mm	1.18 (-0.28,2.64)	-0.01 (-0.05,0.03)	0.23 (-0.42,0.87)	0	0.71		
Prevalence (% positive)	rain < 415 mm	15.20 (6.87,23.52)	-0.43 (-0.65,-0.21)	12.40 (6.13,18.68)	0.06	<0.0001		
	415 mm <rain<950 mm	66.60 (37.24,95.95)	-3.17 (-3.97,-2.36)	106.00 (93.94,117.47)	0.48	<0.0001	0.75	16.52%
	rain > 950 mm	36.00 (-14.86,86.81)	1.42 (-0.11,2.96)	0.45 (-21.88,22.77)	0.02	0.19		
Immunity index (unitless 0 to 1)	rain < 415 mm	0.73 (0.62,0.84)	-0.02 (-0.02,-0.02)	0.03 (-0.06,0.11)	0.24	<0.0001		
	415 mm <rain<950 mm	1.89 (1.61,2.18)	-0.06 (-0.07,-0.06)	0.73 (0.61,0.84)	0.53	<0.0001	0.74	0.16
	rain > 950 mm	1.16 (0.72,1.60)	-0.02 (-0.03,-0.00)	0.14 (-0.06,0.33)	0.05	0.01		

Supplementary Table 4: Summary of data sources

	Data source	Spatial resolution	Temporal resolution	Reference
Baseline Climatology				
temperature	CRU TS 3.21	0.5 x 0.5 degree	1 month 1901-2012	35
rainfall	CRU TS 3.21	0.5 x 0.5 degree	1 month 1901-2012	35
Meteorological Inputs for HYDREMATS Simulation				
precipitation	CMORPH version 1.0	~8km	30 min 1998-present	1
temperature	ERA-Interim	.75 x .75 degree	3 hour 1979-present	8
wind speed	ERA-Interim	.75 x .75 degree	3 hour 1979-present	8
wind direction	ERA-Interim	.75 x .75 degree	3 hour 1979-present	8
surface radiation	ERA-Interim	.75 x .75 degree	3 hour 1979-present	8
Other model inputs				
soil type	Harmonized World Soil Database	~1km	Static	10
vegetation	University of Maryland Landcover	1km	Static	9
topography	Computed from Envisat synthetic aperture radar and ground survey	10 m	Static	36
household locations	Quickbird image	0.6 m	Static	26

Supplementary Table 5: Performance of CMIP5 Climate Models

Model Name	Rainfall Score			Temperature Score			Total
	Zone 1	**Zone 2**	**Zone 3**	**Zone 1**	**Zone 2**	**Zone 3**	
BNU-ESM	1	1	1	1	1	1	6
MIROC5	1	1		1	1	1	5
MPI-ESM-MR	1		1	1	1		4
CANESM2				1	1	1	3
CCSM4	1	1	1				3
FGOALS-g2	-1	1		1	1		2
CESM1-CAM5		1	1				2
MIROC-ESM-CHEM						1	1
FIO-ESM	1						1
BCC-CSM1-1						1	1
CNRM-CM5	-1	1	1				1
CSIRO-Mk3-6-0	-1	-1		1	1	1	1
CMCC-CM							0
GFDL-CM3							0
GISS-E2-H						-1	-1
HadGEM2-AO				-1			-1
ACCESS		-1	-1				-2
MRI-CGCM3		-1	-1		-1		-3
EC-EARTH	-1		1	-1	-1	-1	-3
IPSL-CM5A-MR				-1	-1	-1	-3
GFDL-ESM2M	-1	-1	-1				-3
inmcm4	1		-1	-1	-1	-1	-3
HadGEM2-CC		-1	-1	-1	-1	-1	-5

Supplementary Information References

1 Joyce, R. J., Janowiak, J. E., Arkin, P. A. & Xie, P. CMORPH: A method that produces global precipitation estimates from passive microwave and infrared data at high spatial and temporal resolution. *Journal of Hydrometeorology* **5**, 487-503 (2004).

2 Serrat‐Capdevila, A., Valdes, J. B. & Stakhiv, E. Z. Water management applications for satellite precipitation products: Synthesis and recommendations. *JAWRA Journal of the American Water Resources Association* **50**, 509-525 (2014).

3 Gosset, M., Viarre, J., Quantin, G. & Alcoba, M. Evaluation of several rainfall products used for hydrological applications over West Africa using two high‐resolution gauge networks. *Quarterly Journal of the Royal Meteorological Society* **139**, 923-940 (2013).

4 Yamana, T. K. & Eltahir, E. A. B. On the use of satellite-based estimates of rainfall temporal distribution to simulate the potential for malaria transmission in rural Africa. *Water Resources Research* **47**, W02540 (2011).

5 Wolff, D. B. *et al.* Ground validation for the tropical rainfall measuring mission (TRMM). *Journal of Atmospheric and Oceanic Technology* **22**, 365-380 (2005).

6 De Vera, A. & Terra, R. Combining CMORPH and rain gauges observations over the Rio Negro Basin. *Journal of Hydrometeorology* **13**, 1799-1809 (2012).

7 Guilloteau, C. *et al.* Impacts of satellite-based rainfall products on predicting spatial patterns of the Rift Valley Fever vectors. *Journal of Hydrometeorology* (2014).

8 Dee, D. P. *et al.* The ERA-Interim reanalysis: configuration and performance of the data assimilation system. *Quarterly Journal of the Royal Meteorological Society* **137**, 553-597, doi:10.1002/qj.828 (2011).

9 Hansen, M. C., DeFries, R. S., Townshend, J. R. G. & Sohlberg, R. Global land cover classification at 1 km spatial resolution using a classification tree approach. *International Journal of Remote Sensing* **21**, 1331-1364 (2000).

10 Nachtergaele, F. *et al.* Harmonized world soil database. *Food and Agriculture Organization of the United Nations* (2008).

11 Morin, J. Soil crusting and sealing. Soil tillage in Africa: needs and challenges. *FAO Soils Bulletin (FAO)* **69**, 41-41-67 (1993).

12 Yamana, T. K. & Eltahir, E. A. B. Projected impacts of climate change on environmental suitability for malaria transmission in West Africa. *Environ Health Perspect* **121**, 1179-1186 (2013).

13 Cook, K. H. & Vizy, E. K. Coupled model simulations of the West African monsoon system: Twentieth-and twenty-first-century simulations. *Journal of Climate* **19**, 3681-3703 (2006).

14 Roehrig, R., Bouniol, D., Guichard, F., Hourdin, F. & Redelsperger, J.-L. The present and future of the West African monsoon: a process-oriented assessment of CMIP5 simulations along the AMMA transect. *Journal of Climate* (2013).

15 Druyan, L. M. Studies of 21st‐century precipitation trends over West Africa. *International Journal of Climatology* **31**, 1415-1424 (2011).

16 Crétat, J., Vizy, E. K. & Cook, K. H. How well are daily intense rainfall events captured by current climate models over Africa? *Climate Dynamics* **42**, 2691-2711, doi:10.1007/s00382-013-1796-7 (2013).

17 Bomblies, A. Modeling the role of rainfall patterns in seasonal malaria transmission. *Climatic Change* **112**, 673-685 (2012).

18 Bomblies, A. Agent-based modeling of malaria vectors: the importance of spatial simulation. *Parasit Vectors* **7**, 1-10 (2014).
19 Mote, P. W. & Salathe Jr, E. P. Future climate in the Pacific Northwest. *Climatic Change* **102**, 29-50 (2010).
20 Horton, R. M. *et al.* Climate hazard assessment for stakeholder adaptation planning in New York City. *Journal of Applied Meteorology and Climatology* **50**, 2247-2266 (2011).
21 Hay, L. E., Wilby, R. L. & Leavesley, G. H. (Wiley Online Library, 2000).
22 Seth, A. *et al.* CMIP5 projected changes in the annual cycle of precipitation in monsoon regions. *Journal of Climate* **26**, 7328-7351 (2013).
23 Biasutti, M. & Sobel, A. H. Delayed Sahel rainfall and global seasonal cycle in a warmer climate. *Geophysical Research Letters* **36** (2009).
24 Biasutti, M. Forced Sahel rainfall trends in the CMIP5 archive. *Journal of Geophysical Research: Atmospheres* **118**, 1613-1623 (2013).
25 Wang, G. & Alo, C. A. Changes in precipitation seasonality in West Africa predicted by RegCM3 and the impact of dynamic vegetation feedback. *International Journal of Geophysics* **2012** (2012).
26 Bomblies, A., Duchemin, J. B. & Eltahir, E. A. B. Hydrology of malaria: Model development and application to a Sahelian village. *Water Resour.Res* **44** (2008).
27 Bomblies, A., Duchemin, J. B. & Eltahir, E. A. B. A mechanistic approach for accurate simulation of village-scale malaria transmission. *Malaria Journal* **8**, 223 (2009).
28 Yamana, T. K., Bomblies, A., Laminou, I. M., Duchemin, J.-B. & Eltahir, E. A. Linking environmental variability to village-scale malaria transmission using a simple immunity model. *Parasites & Vectors* **6**, 226 (2013).
29 Beier, J. C., Killeen, G. F. & Githure, J. I. Short report: entomologic inoculation rates and Plasmodium falciparum malaria prevalence in Africa. *The American Journal of Tropical Medicine and Hygiene* **61**, 109-113 (1999).
30 Gething, P. W. *et al.* A new world malaria map: Plasmodium falciparum endemicity in 2010. *Malar J* **10**, 1475-2875 (2011).
31 Molineaux, L. & Gramiccia, G. *The Garki Project*. (World Health Organization, 1980).
32 Omer, S. M. & Cloudsley-Thompson, J. L. Survival of female Anopheles gambiae Giles through a 9-month dry season in Sudan. *Bulletin of the World Health Organization* **42**, 319 (1970).
33 Sultan, B. *et al.* Robust features of future climate change impacts on sorghum yields in West Africa. *Environmental Research Letters* **9**, 104006 (2014).
34 Lee, J.-Y. & Wang, B. Future change of global monsoon in the CMIP5. *Climate Dynamics* **42**, 101-119, doi:10.1007/s00382-012-1564-0 (2012).
35 Mitchell, T. D. & Jones, P. D. An improved method of constructing a database of monthly climate observations and associated high-resolution grids. *International Journal of Climatology* **25**, 693-712, doi:10.1002/joc.1181 (2005).
36 Toutin, T. & Gray, L. State-of-the-art of elevation extraction from satellite SAR data. *ISPRS Journal of Photogrammetry and Remote Sensing* **55**, 13-33 (2000).